

Spatial Transcriptomics Analysis of Spatially Dense Gene Expression Prediction

Ruikun Zhang¹, Yan Yang², and Liyuan Pan¹

¹ School of Computer Science & Technology, Beijing Institute of Technology

² Biological Data Science Institute, The Australian National University
{ruikun.zhang}@bit.edu.cn

Abstract. Spatial transcriptomics (ST) measures gene expression at fine-grained spatial resolution, offering insights into tissue molecular landscapes. Previous methods for spatial gene expression prediction usually crop spots of interest from pathology tissue slide images, and learn a model that maps each spot to a single gene expression profile. However, it fundamentally loses spatial resolution of gene expression: 1) each spot often contains multiple cells with distinct gene expression; 2) spots are cropped at fixed resolutions, limiting the ability to predict gene expression at varying spatial scales. To address these limitations, this paper presents PixNet, a dense prediction network capable of predicting spatially resolved gene expression across spots of varying sizes and scales directly from pathology images. Different from previous methods that map individual spots to gene expression values, we generate a dense continuous gene expression map from the pathology image, and aggregate values within spots of interest to predict the gene expression. Our PixNet outperforms state-of-the-art methods on 3 common ST datasets, while showing superior performance in predicting gene expression across multiple spatial scales. The source code will be publicly available.

Keywords: Spatial transcriptomics · Computational pathology · Gene expression prediction · Tissue slide image · Pixel-level prediction.

1 Introduction

Spatially profiling gene expression with spatial transcriptomics (ST) is clinically beneficial, but its acquisition remains expensive and technically inefficient. Therefore, predicting spatial gene expression from more readily available and cost-effective pathology slide images has been widely studied [10,15,18,20,17,6,19]. To preserve spatial information, the community has formulated the prediction problem as a regression task, mapping a spot of interest from pathology slide images to corresponding gene expression.

Formally, past works approach the problem by cropping spots with measured gene expression in the datasets, and train a network with the processed datasets for the prediction problem. Various networks have been explored: either fine-tuning pretrained networks by leveraging foundation models pretrained on large

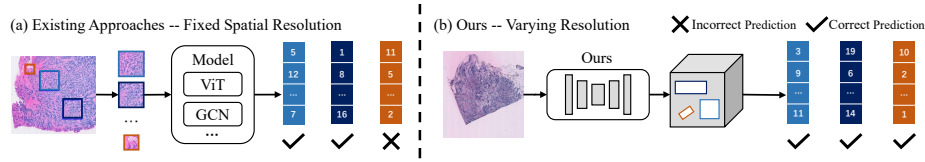


Fig. 1: Overview of fields. (a) Existing approaches treat spatial gene expression prediction as a regression problem, training various networks on fixed crops from a slide image. (b) Our method formulates it as a dense prediction task, generating a gene expression map and aggregating values within spots of interest.

datasets [18,20] or designing multi-scale [6] or graph network-based models [19] for leveraging the spatial context of the slide image to improve the prediction performance. Refer to Fig. 1 (a) for a summary. While these approaches have shown promising results, they fundamentally contradict the goal of predicting spatially resolved gene expression. Specifically, spots are usually cropped at sizes exceeding $100 \mu\text{m}$ to provide sufficient visual and spatial information to the network. It aggregates features from multiple cells within a single spot, mapping a fixed crop to gene expression, which results in a loss of spatial resolution and capability of predicting spatially resolved gene expression.

Moreover, past methods are designed for spots with a fixed scale and size. However, in practice, there is the need for gene expression prediction at varying spatial resolutions and spot sizes, limiting the adaptability of these methods to real-world applications. For example, a model trained to predict gene expression from $100 \mu\text{m}$ spots struggles to generalize when applied to $2 \mu\text{m}$ spots, as it usually relies on larger spot sizes to capture spatial context from the slide image for prediction. Furthermore, the $2 \mu\text{m}$ spots approximate single-cell resolution (*i.e.*, the finest level of detail desired in spatial transcriptomics [4]). However, in image space, it usually corresponds to only 20 pixels. This resolution constraint further restricts the applicability of previous methods to emerging ST technologies, such as Visium HD, which provides spatial gene expression at $2 \mu\text{m}$ spots. The need for a sufficiently large amount of visual information makes it challenging for them to adapt to these advancements.

To address these challenges, this paper reformulates spatial gene expression prediction from a slide image as a dense prediction task. We introduce PixNet, a model that maps the entire slide image to a dense gene expression map. For any spots of interest, the predicted gene expression is obtained by aggregating values from the corresponding region in the dense gene expression map. Fig. 1 (b) illustrates the overall idea. To generate the gene expression map, we leverage the multi-scale nature of slide images [6]. Because slide images contain features at varying spatial scales, we extract a pyramidal feature map from the slide image, and progressively decode it into a high-resolution gene expression map, capturing hierarchical features for densely predicting the spatial gene expression. In training, we optimize the network by a sparse loss module that provides supervision signals only at spots with measured ground-truth gene expression, ac-

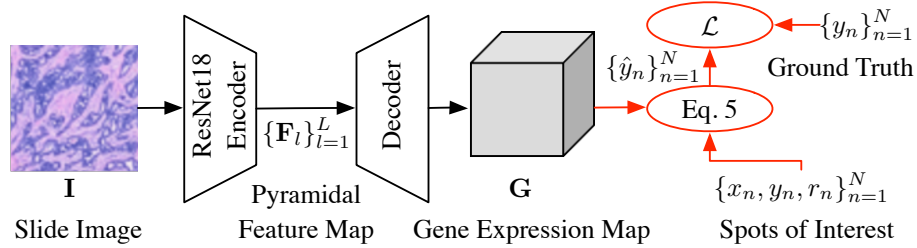


Fig. 2: Overview of our framework. We extract a pyramidal feature map $\{\mathbf{F}_l\}_{l=1}^L$ from a slide image **I** and progressively decode them into a gene expression map **G**. The predicted gene expression values $\{\hat{y}_n\}_{n=1}^N$ are aggregated (Eq. 5) from **G** based on the positions and radii of spots of interest. The loss \mathcal{L} is computed sparsely on spots with ground truth gene expression $\{y_n\}_{n=1}^N$ during training.

commodating the sparsity of spatial transcriptomics data. With this generalized approach, our network is capable of accurately predicting spatial gene expression across multiple scales at varying sizes. We evaluate our method on 3 common ST datasets and demonstrate its effectiveness in predicting gene expression at scales and spot sizes different from those seen during training, outperforming previous methods. For example, when trained on $100 \mu\text{m}$ spots, our network generalizes to gene expression prediction at single-cell resolution (*i.e.*, $2 \mu\text{m}$) with a Pearson correlation coefficient of 0.160, which is 26.2% higher than past best approach.

2 Method

Overview. Given a slide image $\mathbf{I} \in \mathbb{R}^{H \times W \times 3}$ and N spots $\{x_n, y_n\}_{n=1}^N$, each spot is centered at location (x_n, y_n) on the slide image with a circular radius r_n and is paired with expression $\mathbf{y}_n \in \mathbb{R}^M$ for M genes. H and W are height and width of the slide image. We train a network to predict the gene expression with three steps: 1) the slide image is encoded into L levels of pyramidal feature map $\{\mathbf{F}_l\}_{l=1}^L$; 2) the pyramidal feature map $\{\mathbf{F}_l\}_{l=1}^L$ is decoded progressively into a dense gene expression map $\mathbf{G} \in \mathbb{R}^{H \times W \times M}$; 3) the gene expression \hat{y}_n is predicted for the spot centered at (x_n, y_n) by summing over the values within a circular region of radius r_n in the dense gene expression map **G**. During training, $\{\hat{y}_n\}_{n=1}^N$ is optimized with the ground truth gene expression $\{\mathbf{y}_n\}_{n=1}^N$, forming our sparse loss module. During testing, the spot location (x'_n, y'_n) and radius r'_n can be varied dynamically, allowing for flexible gene expression prediction across different spatial resolutions and spot sizes. An overview is in Fig. 2.

2.1 Pyramidal Feature Extraction

To capture the features with varying scales and sizes in the slide image **I**, we extract a pyramidal feature map using a ResNet18 encoder pretrained on a

large slide image dataset. The encoder consists of L sequential feature extraction stages and can be expressed as

$$\mathbf{F}_L = \text{ResLayer}_L \circ \text{ResLayer}_{L-1} \circ \cdots \circ \text{ResLayer}_1(\mathbf{I}), \quad (1)$$

where $\text{ResLayer}_l(\cdot)$ is the feature extraction layer at stage l . The set of features $\{\mathbf{F}_l\}_{l=1}^L$ is obtained from the L stages and constitutes our pyramidal feature representation, where

$$\mathbf{F}_l = \begin{cases} \text{ResLayer}_l(\mathbf{I}), & \text{for } l = 1 \\ \text{ResLayer}_l \circ \cdots \circ \text{ResLayer}_1(\mathbf{I}), & \text{for } l \geq 2. \end{cases} \quad (2)$$

2.2 Gene Expression Map Decoding

We facilitate the interactions among pyramidal feature map $\{\mathbf{F}_l\}_{l=1}^L$ to progressively decode a gene expression map \mathbf{G} . Our decoder network has $L - 1$ layer, and follows a u-net style. Setting \mathbf{F}_L as the initial decoder feature \mathbf{D}_0 , we iteratively decode the pyramidal feature map $\{\mathbf{F}_l\}_{l=1}^L$. At each stage $1 \leq l \leq L - 1$ stages, we upsample \mathbf{D}_{l-1} using a deconvolution layer $\text{Dconv}(\cdot)$ and fuse it with \mathbf{F}_l through a convolution-based two-layer feedforward block $\text{DFFN}(\cdot)$ [8]. The decoded feature \mathbf{D}_l is

$$\mathbf{D}_l = \text{DFFN}(\text{Dconv}(\mathbf{D}_{l-1}) + \delta \cdot \mathbf{F}_l), \quad (3)$$

where δ is a learnable scale factor that balances the contribution of \mathbf{F}_l during decoding. For the last feature \mathbf{D}_{L-1} , it is forwarded to a linear layer $\text{Linear}(\cdot)$, and resized to match the dimensions of the slide image \mathbf{I} using $\text{Resize}(\cdot)$ to predict the gene expression map \mathbf{G} ,

$$\mathbf{G} = \text{Resize}(\text{Linear}(\mathbf{D}_{L-1})). \quad (4)$$

2.3 Gene Expression Prediction

For a spot with location (x_n, y_n) and radius r_n on the slide image \mathbf{I} , the predicted gene expression \hat{y}_n is

$$\hat{y}_n = \sum_{\Delta x, \Delta y} \mathbf{G}(\Delta x, \Delta y), \quad (5)$$

where the sum enumeration all positions $(\Delta x, \Delta y)$ on the domain of $(\Delta x - x_n)^2 + (\Delta y - y_n)^2 \leq r_n^2$, and $\mathbf{G}(\Delta x, \Delta y)$ denotes the predicted gene expression at position $(\Delta x, \Delta y)$. This aggregation effectively pools the gene expression values within the spot, yielding a robust prediction for each spot.

Table 1: Quantitative gene expression prediction comparisons with state-of-the-art methods on three datasets. The best-performing method is highlighted in bold, and the second-best method is underlined.

Method	MSE (\downarrow)	MAE (\downarrow)	PCC@F (\uparrow)	PCC@S (\uparrow)	PCC@M (\uparrow)
Experiments on the breast cancer Visium HD dataset.					
STNet [10]	0.269 \pm 0.03	0.482 \pm 0.05	-0.009 \pm 0.05	-0.001 \pm 0.06	-0.001 \pm 0.06
HistoGene [15]	0.265 \pm 0.02	0.438 \pm 0.05	0.089 \pm 0.07	0.159 \pm 0.10	0.157 \pm 0.10
EGN [18]	0.264 \pm 0.03	0.413 \pm 0.03	0.102 \pm 0.03	0.166 \pm 0.10	0.161 \pm 0.08
EGGN [20]	0.241 \pm 0.02	0.423 \pm 0.05	0.143 \pm 0.02	0.209 \pm 0.05	0.200 \pm 0.06
BLEEP [17]	0.247 \pm 0.05	0.435 \pm 0.05	0.157 \pm 0.03	0.216 \pm 0.08	0.205 \pm 0.08
TRIPLEX [6]	0.259 \pm 0.04	0.432 \pm 0.08	0.122 \pm 0.03	0.200 \pm 0.04	0.199 \pm 0.07
SGN [19]	<u>0.230</u> \pm 0.03	<u>0.358</u> \pm 0.06	<u>0.173</u> \pm 0.07	<u>0.227</u> \pm 0.04	<u>0.226</u> \pm 0.02
Ours	0.176 \pm 0.02	0.299 \pm 0.05	0.179 \pm 0.02	0.266 \pm 0.03	0.268 \pm 0.02
Experiments on the brain cancer Visium HD dataset.					
STNet [10]	0.282 \pm 0.03	0.514 \pm 0.05	-0.002 \pm 0.05	0.046 \pm 0.06	0.044 \pm 0.06
HistoGene [15]	0.279 \pm 0.02	0.457 \pm 0.05	0.100 \pm 0.07	0.171 \pm 0.10	0.166 \pm 0.10
EGN [18]	0.277 \pm 0.03	0.463 \pm 0.03	0.096 \pm 0.03	0.177 \pm 0.10	0.171 \pm 0.08
EGGN [20]	0.259 \pm 0.02	0.459 \pm 0.05	0.131 \pm 0.02	0.195 \pm 0.05	0.191 \pm 0.06
BLEEP [17]	0.243 \pm 0.05	0.477 \pm 0.05	0.121 \pm 0.03	0.189 \pm 0.08	0.186 \pm 0.08
TRIPLEX [6]	0.257 \pm 0.04	0.462 \pm 0.08	0.132 \pm 0.03	0.195 \pm 0.04	0.188 \pm 0.07
SGN [19]	<u>0.228</u> \pm 0.03	<u>0.447</u> \pm 0.06	<u>0.133</u> \pm 0.07	<u>0.199</u> \pm 0.04	<u>0.195</u> \pm 0.02
Ours	0.223 \pm 0.02	0.407 \pm 0.05	0.152 \pm 0.02	0.213 \pm 0.03	0.202 \pm 0.02
Experiments on the STNet [10] dataset.					
STNet [10]	0.209 \pm 0.02	0.502 \pm 0.05	0.005 \pm 0.06	0.092 \pm 0.07	0.093 \pm 0.06
HistoGene [15]	0.314 \pm 0.09	0.591 \pm 0.12	0.097 \pm 0.10	0.126 \pm 0.11	0.219 \pm 0.12
EGN [18]	0.192 \pm 0.02	0.449 \pm 0.04	0.106 \pm 0.05	0.221 \pm 0.07	0.203 \pm 0.09
EGGN [20]	0.189 \pm 0.03	0.424 \pm 0.06	0.184 \pm 0.05	0.305 \pm 0.05	0.292 \pm 0.06
BLEEP [17]	0.235 \pm 0.02	0.451 \pm 0.05	0.155 \pm 0.05	0.208 \pm 0.05	0.193 \pm 0.10
TRIPLEX [6]	0.202 \pm 0.02	0.413 \pm 0.03	0.159 \pm 0.04	<u>0.364</u> \pm 0.05	<u>0.352</u> \pm 0.10
SGN [19]	0.186 \pm 0.02	<u>0.388</u> \pm 0.05	0.179 \pm 0.05	0.289 \pm 0.06	0.269 \pm 0.07
Ours	<u>0.188</u> \pm 0.04	0.377 \pm 0.04	<u>0.181</u> \pm 0.03	0.369 \pm 0.02	0.362 \pm 0.05

2.4 Loss Function

We sparsely supervise the predicted gene expression map \mathbf{G} with the mean square error \mathcal{L}_{mse} and batch-wise Pearson correlation coefficient (PCC) loss \mathcal{L}_{pcc} . The loss function penalizes deviations of aggregated gene expression $\{\hat{y}_n\}_{n=1}^N$ from the ground truth gene expression $\{y_n\}_{n=1}^N$, and encourages a correlation between them. The overall training loss \mathcal{L} is

$$\mathcal{L} = \mathcal{L}_{\text{mse}} + \lambda \cdot \mathcal{L}_{\text{pcc}} , \quad (6)$$

where λ is a hyperparameter that controls the relative importance of the PCC loss compared to the mean square error.

Table 2: Performance generalization. All models are trained on the STNet [10] dataset (with spot size $100\mu\text{m}$), and tested on the breast cancer Visium HD dataset with varying spot sizes ($2\mu\text{m}$, $8\mu\text{m}$, and $16\mu\text{m}$) and slide images from different environments. The standard deviation is not displayed due to space limitations.

Method	$2\mu\text{m}$			$8\mu\text{m}$			$16\mu\text{m}$		
	MSE	MAE	PCC@M	MSE	MAE	PCC@M	MSE	MAE	PCC@M
STNet [10]	0.420	0.515	0.000	0.397	0.498	0.002	0.395	0.501	0.005
HistoGene [15]	0.388	0.501	0.088	0.389	0.500	0.093	0.373	0.485	0.097
EGN [18]	0.371	0.492	0.091	0.377	0.479	0.087	0.365	0.481	0.100
EGGN [20]	0.368	0.483	0.087	0.372	0.499	0.088	0.361	0.487	0.102
BLEEP [17]	0.323	0.441	0.115	0.302	0.431	0.127	0.301	0.435	<u>0.125</u>
TRIPLEX [6]	0.365	0.488	0.092	0.355	0.451	0.100	0.356	0.457	0.099
SGN [19]	<u>0.303</u>	<u>0.437</u>	<u>0.118</u>	<u>0.289</u>	<u>0.422</u>	<u>0.136</u>	<u>0.286</u>	<u>0.431</u>	0.123
Ours	0.270	0.415	0.160	0.245	0.411	0.183	0.240	0.398	0.190

3 Experiment

Datasets. We experiment with three common datasets: 1) STNet dataset [10] that has 68 slide images with 30K spots on $100\mu\text{m}$; 2) Breast cancer Visium HD dataset, providing 2 slide images with 18.7M, 1.17M, and 294K spots on $2\mu\text{m}$, $8\mu\text{m}$, and $16\mu\text{m}$; 3) Brain cancer Visium HD dataset with 14.2M, 889K, and 223K spots on $2\mu\text{m}$, $8\mu\text{m}$, and $16\mu\text{m}$ from 2 slide images; We follow the preprocessing and cross-fold validation protocols outlined in [20,19]. The Visium HD dataset is downloaded from 10xProteomic³, including the Visium HD Spatial Gene Expression Library, Human Breast Cancer; and Visium HD Spatial Gene Expression Library, Mouse Brain.

Evaluation Metrics. Our method is evaluated using the following metrics: mean squared error (MSE), mean absolute error (MAE), first quartile of Pearson correlation coefficient (PCC@F), median of Pearson correlation coefficient (PCC@S), and mean of Pearson correlation coefficient (PCC@M).

Implementation Details. We implement PixNet in the *PyTorch* framework [9,16]. We train it with the Adam optimizer for 500 epochs, using a learning rate of 5×10^{-4} and a weight decay of 1×10^{-4} . We employ hidden dimensions of 512 in our decoder. We set λ to 0.5. Following the approach in [10], we select the 250 genes with the highest mean expression across the dataset as prediction targets. The gene expression values are normalized by dividing by the sum of expressions in each spot, followed by a log transformation [6].

3.1 Experimental Result

We compare our method with state-of-the-art methods on the STNet [10], Breast cancer Visium HD, and Brain cancer Visium HD datasets in Tab. 1. Though our

³ <https://www.10xgenomics.com/resources/datasets>

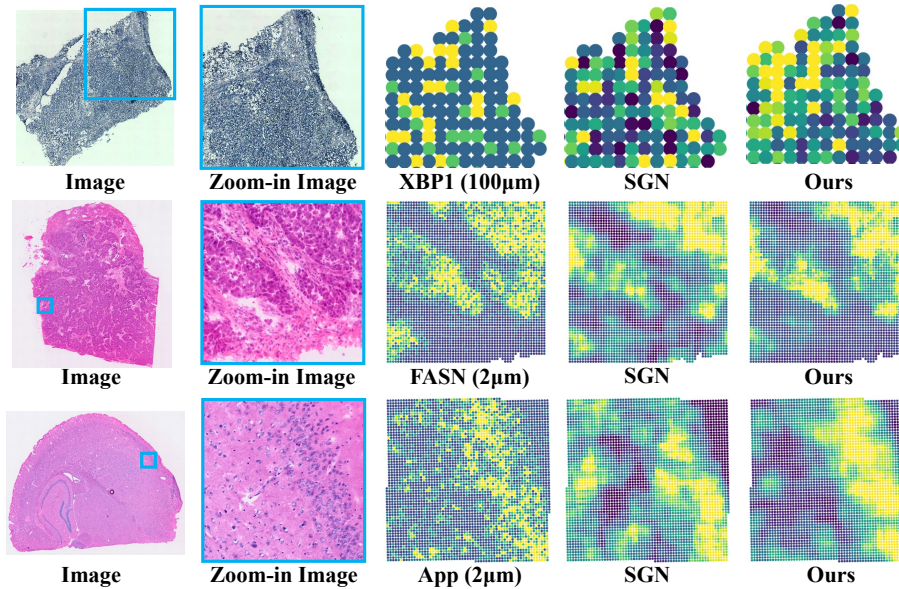


Fig. 3: Examples of predicted expression of gene types that are related to cancers [10,21,14,12,3,13,1]. From left to right, we show the slide image, ground truth gene expression, and predictions from various methods are shown for regions cropped from the colored boxes in the slide image.

method has a lower MSE than SGN [19] on the STNet dataset, our method consistently demonstrates the leading PCC-based performance on the three datasets. This is particularly important for gene expression prediction, as it verifies the model’s ability to effectively capture relative variations in gene expression. For instance, on the breast cancer Visium HD dataset, our method achieves a PCC@M of 0.268, which is a 18.6% improvement over the previous state-of-the-art method, SGN (0.226 PCC@M).

We show qualitative examples comparing competitive methods for gene expression prediction in Fig. 3. Our method has a visual pattern that is more similar to the ground truth gene expression.

3.2 Ablation Study

Generalization. Our network is able to generalize to the prediction of spots with different sizes than those used during training. We compare our performance with state-of-the-art methods to evaluate its robustness and adaptability in cross-spot sizes in Tab. 2. We significantly outperform the previous state-of-the-art method (SGN [19]), which is trained to predict gene expression from fixed spots. However, our method generalizes the problem to dense prediction, enabling more flexible and accurate gene expression estimation.

Table 3: Ablation study of gene expression measured for different spot sizes used in training.

$16\ \mu m$	Bin size		MSE(\downarrow)	MAE(\downarrow)	PCC@M(\uparrow)
	$8\ \mu m$	$2\ \mu m$			
✓	✗	✗	0.213 \pm 0.03	0.374 \pm 0.04	0.179 \pm 0.06
✗	✓	✗	0.209 \pm 0.03	0.369 \pm 0.05	0.187 \pm 0.06
✗	✗	✓	0.185 \pm 0.02	0.331 \pm 0.04	0.238 \pm 0.04
✓	✓	✗	0.201 \pm 0.04	0.374 \pm 0.06	0.200 \pm 0.07
✓	✓	✓	0.177\pm0.02	0.301\pm0.05	0.266\pm0.02

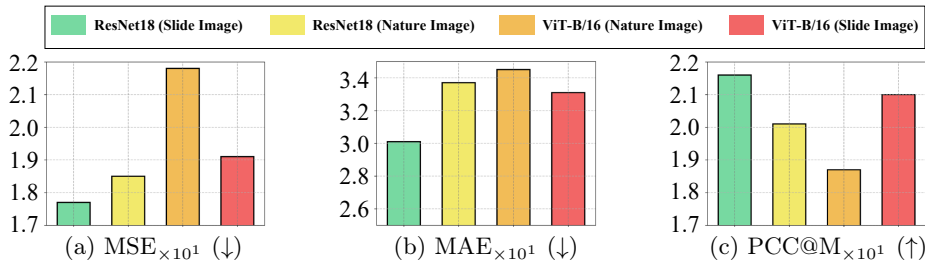


Fig. 4: Ablation study of the pretrained image encoder [7,11,5,2].

Foundation Encoder. We ablate the pretrained image encoder used for extracting our pyramidal feature map. We explore ResNet18 [11,7] and ViT-B/16 [5,2] pretrained on nature images and slide images. The results on the breast cancer Visium HD dataset shown in Fig. 4. Using the ResNet18 model pretrained on slide images [7] achieves the best performance.

Spot Size. We conduct an ablation study on gene expression for spots of different sizes on the breast cancer Visium HD dataset in Tab. 3. When excluding the $2\ \mu m$ spots, there is a significant drop in model performance. This spot size usually corresponds to a single cell, which produces gene expression. These findings highlight the importance of enabling the network to explore the expression of each individual cell. The best performance is achieved when all data are utilized.

4 Conclusion

In this paper, we introduce PixNet, for densely predicting the spatial gene expression from slide images. Our method generates a dense gene expression map from the slide image while applying sparse supervision only to spots with available ground truth gene expression. This approach enables our method to generalize effectively, allowing for accurate gene expression prediction across spots of varying scales and sizes. Extensive experiments demonstrate that our PixNet framework performs competitively compared to state-of-the-art gene expression prediction methods.

References

1. Chaturvedi, S., Biswas, M., Sadhukhan, S., Sonawane, A.: Role of *egfr* and *fasn* in breast cancer progression. *Journal of Cell Communication and Signaling* **17**(4), 1249–1282 (2023)
2. Chen, R.J., Ding, T., Lu, M.Y., Williamson, D.F., Jaume, G., Chen, B., Zhang, A., Shao, D., Song, A.H., Shaban, M., et al.: Towards a general-purpose foundation model for computational pathology. *Nature Medicine* (2024)
3. Chen, S., Chen, J., Hua, X., Sun, Y., Cui, R., Sha, J., Zhu, X.: The emerging role of *xbp1* in cancer. *Biomedicine & Pharmacotherapy* **127**, 110069 (2020)
4. Chen, W.T., Lu, A., Craessaerts, K., Pavie, B., Sala Frigerio, C., Corthout, N., Qian, X., LalÅakovÅa, J., KÅijhnmund, M., Voytyuk, I., Wolfs, L., Mancuso, R., Salta, E., Balusu, S., Snellinx, A., Munck, S., Jurek, A., Fernandez Navarro, J., Saïdo, T.C., Huitinga, I., Lundeberg, J., Fiers, M., De Strooper, B.: Spatial transcriptomics and in situ sequencing to study alzheimerÅs disease. *Cell* **182**(4), 976–991.e19 (2020). <https://doi.org/https://doi.org/10.1016/j.cell.2020.06.038>, <https://www.sciencedirect.com/science/article/pii/S0092867420308151>
5. Cherti, M., Beaumont, R., Wightman, R., Wortsman, M., Ilharco, G., Gordon, C., Schuhmann, C., Schmidt, L., Jitsev, J.: Reproducible scaling laws for contrastive language-image learning. In: *Proceedings of the IEEE/CVF Conference on Computer Vision and Pattern Recognition*. pp. 2818–2829 (2023)
6. Chung, Y., Ha, J.H., Im, K.C., Lee, J.S.: Accurate spatial gene expression prediction by integrating multi-resolution features. In: *Proceedings of the IEEE/CVF Conference on Computer Vision and Pattern Recognition*. pp. 11591–11600 (2024)
7. Ciga, O., Xu, T., Martel, A.L.: Self supervised contrastive learning for digital histopathology. *Machine Learning with Applications* **7**, 100198 (2022)
8. Fan, X., Wang, X., Gao, J., Wang, J., Luo, Z., Liu, R.: Bi-level learning of task-specific decoders for joint registration and one-shot medical image segmentation. In: *Proceedings of the IEEE/CVF Conference on Computer Vision and Pattern Recognition*. pp. 11726–11735 (2024)
9. Fey, M., Lenssen, J.E.: Fast graph representation learning with pytorch geometric. *CoRR* **abs/1903.02428** (2019), <http://arxiv.org/abs/1903.02428>
10. He, B., BergenstrÅhle, L., Stenbeck, L., Abid, A., Andersson, A., Borg, A., Maaskola, J., Lundeberg, J., Zou, J.: Integrating spatial gene expression and breast tumour morphology via deep learning. *Nature Biomedical Engineering* **4**, 1–8 (08 2020). <https://doi.org/10.1038/s41551-020-0578-x>
11. He, K., Zhang, X., Ren, S., Sun, J.: Deep residual learning for image recognition. pp. 770–778 (06 2016). <https://doi.org/10.1109/CVPR.2016.90>
12. Jiang, Y., Yang, L., Jiang, L., Yu, W., Jin, Z., Qiu, Y., Liao, Y., Liu, J., Zhang, H.: X-box binding protein 1 is a potential immunotherapy target in ovarian cancer. *Frontiers in Genetics* **13**, 818917 (2022)
13. Menendez, J.A., Lupu, R.: Fatty acid synthase (*fasn*) as a therapeutic target in breast cancer. *Expert opinion on therapeutic targets* **21**(11), 1001–1016 (2017)
14. Orobets, K.S., Karamyshev, A.L.: Amyloid precursor protein and alzheimerÅs disease. *International journal of molecular sciences* **24**(19), 14794 (2023)
15. Pang, M., Su, K., Li, M.: Leveraging information in spatial transcriptomics to predict super-resolution gene expression from histology images in tumors. *BioRxiv* pp. 2021–11 (2021)

16. Paszke, A., Gross, S., Massa, F., Lerer, A., Bradbury, J., Chanan, G., Killeen, T., Lin, Z., Gimelshein, N., Antiga, L., Desmaison, A., Köpf, A., Yang, E.Z., DeVito, Z., Raison, M., Tejani, A., Chilamkurthy, S., Steiner, B., Fang, L., Bai, J., Chintala, S.: Pytorch: An imperative style, high-performance deep learning library. In: Wallach, H.M., Larochelle, H., Beygelzimer, A., d'Alché-Buc, F., Fox, E.B., Garnett, R. (eds.) *Advances in Neural Information Processing Systems 32: Annual Conference on Neural Information Processing Systems 2019, NeurIPS 2019, December 8-14, 2019, Vancouver, BC, Canada*. pp. 8024–8035 (2019), <https://proceedings.neurips.cc/paper/2019/hash/bdbca288fee7f92f2bfa9f7012727740-Abstract.html>
17. Xie, R., Pang, K., Chung, S., Perciani, C., MacParland, S., Wang, B., Bader, G.: Spatially resolved gene expression prediction from histology images via bimodal contrastive learning. *Advances in Neural Information Processing Systems* **36**, 70626–70637 (2023)
18. Yang, Y., Hossain, M., Stone, E., Rahman, S.: Exemplar guided deep neural network for spatial transcriptomics analysis of gene expression prediction (10 2022)
19. Yang, Y., Hossain, M.Z., Li, X., Rahman, S., Stone, E.: Spatial transcriptomics analysis of zero-shot gene expression prediction. In: *International Conference on Medical Image Computing and Computer-Assisted Intervention*. pp. 492–502. Springer (2024)
20. Yang, Y., Hossain, M.Z., Stone, E., Rahman, S.: Spatial transcriptomics analysis of gene expression prediction using exemplar guided graph neural network. *Pattern Recognition* **145**, 109966 (2024). <https://doi.org/https://doi.org/10.1016/j.patcog.2023.109966>, <https://www.sciencedirect.com/science/article/pii/S0031320323006647>
21. Zhou, Z.d., Chan, C.H.s., Ma, Q.h., Xu, X.h., Xiao, Z.c., Tan, E.K.: The roles of amyloid precursor protein (app) in neurogenesis: Implications to pathogenesis and therapy of alzheimer disease. *Cell adhesion & migration* **5**(4), 280–292 (2011)